9.7 ELASTIC BACKSCATTER LIDAR OBSERVATIONS OF A GUST FRONT PASSAGE OVER WASHINGTON DC ON 7 MAY 2004

Shane D. Mayor*, Bruce M. Morley, Scott M. Spuler, Stephan C. Himmelsbach, Dennis Flanigan, Tammy M. Weckwerth, and Thomas Warner

National Center for Atmospheric Research, Boulder, Colorado

1. INTRODUCTION

Thunderstorm gust fronts, or outflow boundaries, impact society in several significant ways. They can serve as a focusing mechanism for the initiation of new severe storm activity (Weckwerth and Wakimoto, 1992). Gust fronts also pose a hazard in aviation by the strong wind shear associated with them (Fujita and Caracena, 1977). They can have an economic impact also by disrupting the flow of aircraft departures and arrivals. Finally, at least one study links the occurrence of gust fronts with epidemics of asthma in urban areas (Marks et al., 2001). Numerical simulation and prediction of gust fronts are challenging (Straka et al., 1993). Improved observations are known to lead to improved short-term prediction (Wilson et al., 1998) and are needed to test numerical simulations (Liu and Moncrieff, 1996). This paper highlights just one example of how an eye-safe scanning aerosol lidar can provide improved observations. In the future, such a lidar system might serve a role in mesoscale urban observing networks (Dabberdt et al., 2005).

The first deployment of the NCAR Raman-shifted Eye-safe Aerosol Lidar (REAL) occurred in May of 2004 in Washington D.C. (Warner et al., 2007). The lidar was set up on the west bank of the Potomac River for about 10 days. Figure 1 shows a photo of the system at that location. The white shipping container housing the lidar was placed on top of an empty shipping container in order to raise the instrument to a height above the ground where it could scan horizontally over nearby buildings. During the deployment, a gust front, resulting from the outflow of a distant thunderstorm, passed over the region which is also the heart of Washington, D.C.

In this paper, we briefly describe the lidar and its observations of the gust front passage. We show initial attempts to track the leading edge with a wavelet algorithm and determine the velocity vector field of aerosol structures behind the front via a correlation algorithm. In the future, such algorithms should prove useful in studying the structure and dynamics of the leading edge in research programs and provide automatic advanced notice of such a front's arrival time in nowcasting applications.

Figure 1: Photo of the NCAR REAL during deployment in Washington, D.C., in May of 2004.

2. NCAR REAL

The NCAR REAL is described in detail by Mayor and Spuler (2004) and Spuler and Mayor (2005). The instrument is operated by the Earth Observing Laboratory (EOL) of NCAR. Although not yet in the National Science Foundation (NSF) deployment pool, REAL is available for use by the university community by submitting a request to the NSF Atmospheric Sciences Division. The lidar system is unique in that it operates at 1.5-microns wavelength. This wavelength falls within a narrow region of the near-infrared portion of the optical spectrum that offers maximum eye-safety. By operating at this wavelength, a lidar can transmit high pulse energy safely. REAL is eye-safe at 0 meters range for a 10 second unaided stare according to ANSI standards. An additional important feature for lidar operation in urban regions is an invisible beam. Other eye-safe lidars with invisible beams exist, but high-pulse energy operation at 1.5 microns enables the use of an analog direct

* *corresponding author address:* Shane D. Mayor, National Center for Atmospheric Research, P. O. Box 3000, Boulder, CO 80307-3000; *email*: shane@ucar.edu

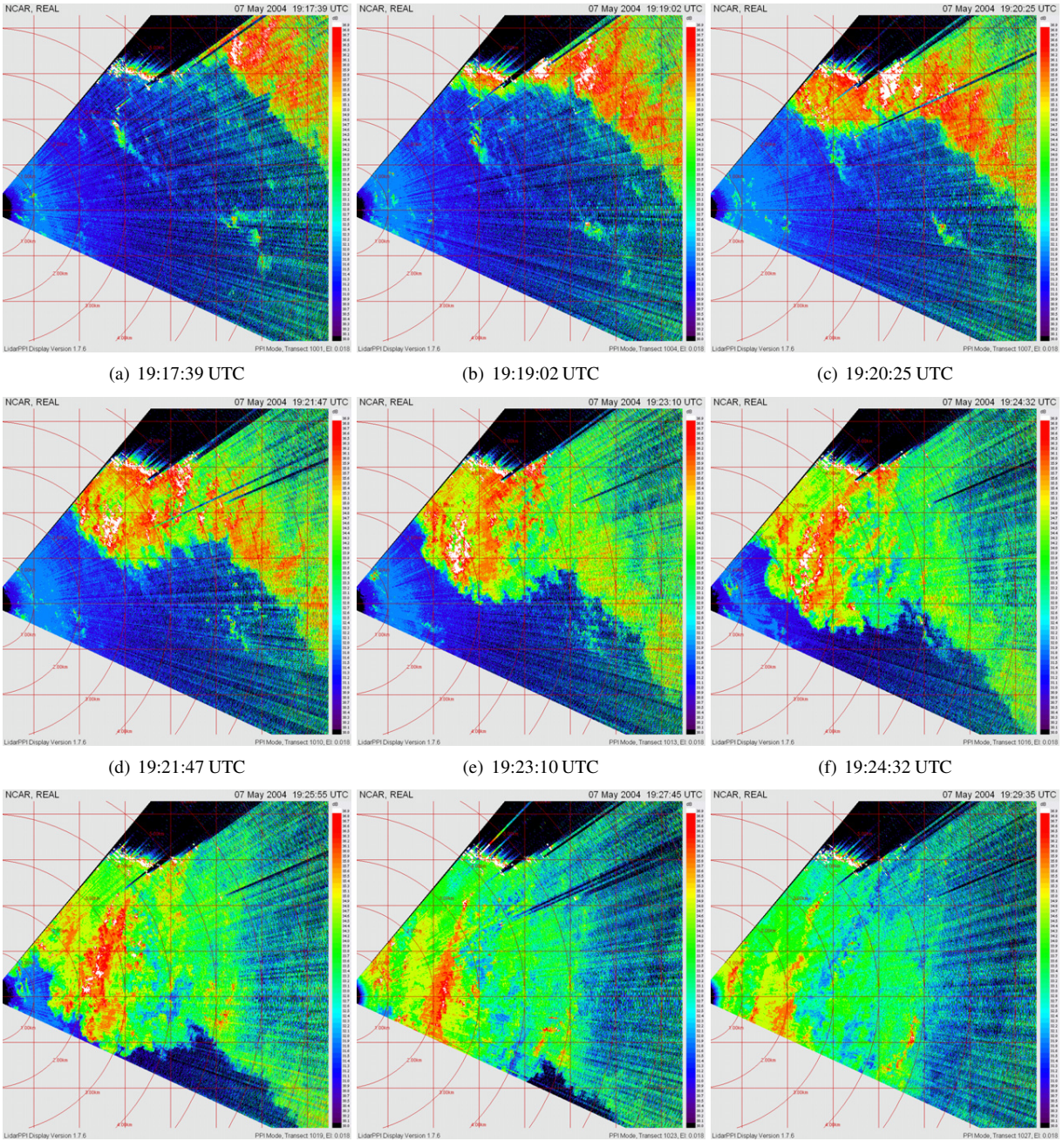

(a) 19:17:39 UTC (b) 19:19:02 UTC (c) 19:20:25 UTC

(d) 19:21:47 UTC (e) 19:23:10 UTC (f) 19:24:32 UTC

(g) 19:25:55 UTC (h) 19:27:45 UTC (i) 19:29:35 UTC

Figure 2: Horizontal scans from the NCAR REAL during the 7 May 2004 gust front passage. The frames shown represent only one-third of all frames available during the period. Range rings and grid lines are in 1 km intervals.

detection receiver and rapid scanning. Rapid scanning enables one to create time-lapse animations of flow as evidenced by variability in the aerosol backscatter. For this experiment, the lidar transmitted 10 laser pulses per second and typically scanned at 4 degrees per second. Backscatter intensity was recorded at 3-meter intervals along each beam, but this digitization rate over-sampled the backscatter signal due to bandwidth limitations of the amplifier electronics. Scans, such as those shown in Fig. 2, are collected approximately every 30 seconds or less. By linking the scan frames together in a digital movie, time-lapse animations of atmospheric flow, just tens of meters above tree-top and roof-top can be created.

Since the May 2004 deployment, REAL has benefited from substantial improvements. They include (1) the ability to run continuously and unattended for periods of several weeks, (2) the ability to interleave the collection of RHI and PPI scans in order to provide horizontal and vertical animations during the same period, (3) backscatter polarization sensitivity (Mayor et al., 2007b), and (4) remote control and near-real-time "Quicklook image" perusal via the internet. A recent field experiment that utilized these new capabilities is described by Mayor et al. (2007a). Final data products are now delivered in NetCDF format and programs have been written in Matlab and IDL to make data access and custom data processing easier.

3. OBSERVATIONS

On the afternoon of 7 May 2004, at approximately 19:20 UTC (14:20 EDT), a gust front passed over the lidar's observing area. The front evidenced itself in the lidar scans as an abrupt increase in aerosol backscatter. Behind the leading edge of the newly arrived airmass, aerosol features lined up with the prevailing north-northeast flow. Figure 2 shows a subset (every third frame) of the lidar scans during that period. Range rings and grid lines are in 1 km intervals. The sequence of images show the progression of the leading edge of the front. In general, the front moved approximately 7 km in 12 minutes, or about 9.7 m s^{-1}. The lidar data show that the shape of the front is complex. Some parts have advanced more rapidly than others. The bright features just beyond 4-km range and casting black shadows at the top edge of the scan are reflections from objects such as buildings and trees.

During this period a surface weather station near the lidar site recorded changes in wind, temperature and humidity. Figures 3 and 4 show time-series of these variables for a 24-minute period. The wind direction shifted from slightly west of north to slightly east of north. The wind speed increased from < 4 m s^{-1} before the arrival

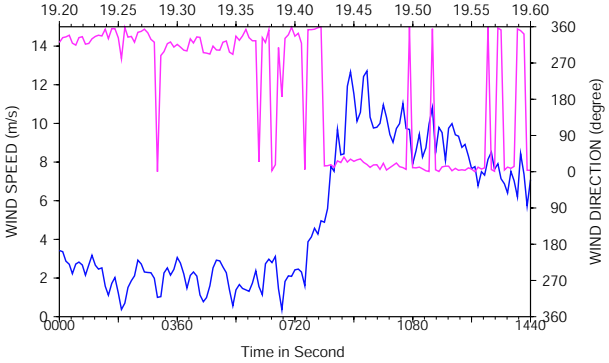

Figure 3: Time series of wind speed (blue line) and direction (magenta line) during the passage of the leading edge of the gust front on 7 May 2004.

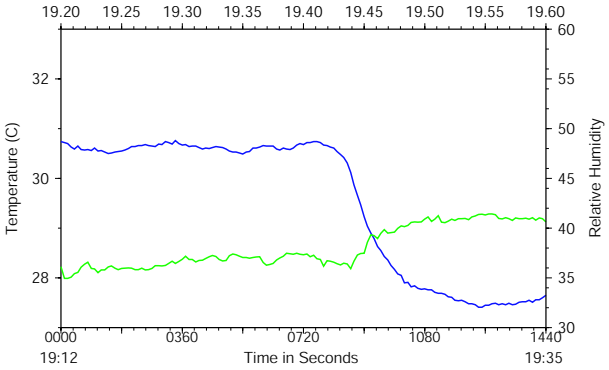

Figure 4: Time series of temperature (blue line) and relative humidity (green line) during the passage of the leading edge of the gust front on 7 May 2004.

of the front to as much as 12 m s^{-1} just behind the front. The temperature decreased from 31°C to 27°C. The relative humidity increased from 36% to 41%. Observers at the lidar site noticed a slight reduction in visibility with the passage of the front but no precipitation.

Figure 5 is a 0.5-degree elevation scan from the Sterling, Virginia, NWS-88D radar. The radar is located about 40 km west-north-west of the lidar's observing area. The images shows an east-west oriented line of enhanced radar reflectivity passing across the lidar's observing area at 19:24 UTC. A region of precipitation is located approximately 20 km to the NE of the lidar. These observations confirm that the phenomena in the lidar data are a gust front and thunderstorm outflow. The lidar and radar provide complimentary observations.

3.1 Wavelets

We applied the Haar wavelet algorithm, described by Davis et al. (2000), to objectively identify the leading

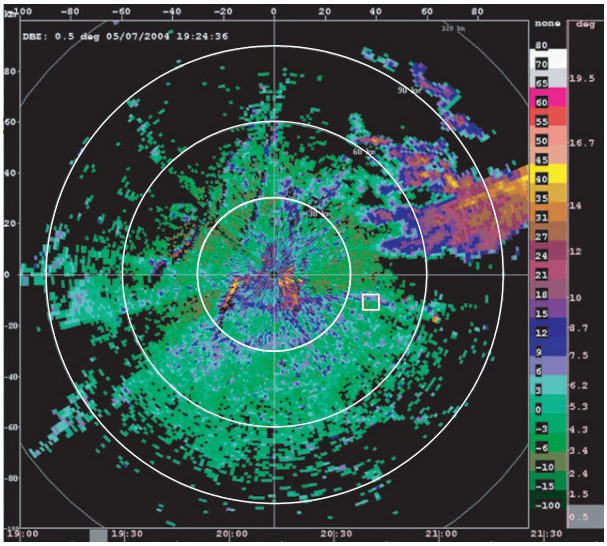

Figure 5: Radar reflectivity at 19:24 UTC from the Sterling, Virginia, WSR88D. Range rings are drawn in 30 km intervals. The image, and others in a time sequence, show an east-west oriented outflow boundary move across the lidar's observing region which is indicated by the small white box located about 40 km ESE of the radar site. The small white box is 6.5 km on a side.

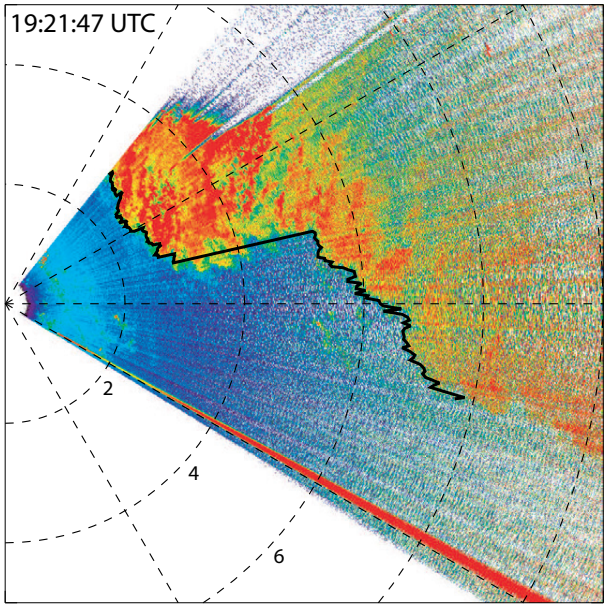

Figure 6: One scan from the lidar with the location of the front (thick black line) as determined by the wavelet algorithm. Range rings are plotted in 2 km intervals.

edge of the gust front. The airmass behind the leading edge of the gust front is evidenced with high aerosol backscattering. The front itself creates a step-like feature in the backscatter data—very similar in gradient to the top edge of an aerosol rich boundary layer in vertically pointing lidar data. Therefore, a Haar wavelet with large (1 km) dilation was applied to each radial beam of backscatter data. Use of a large dilation provides a robust identification of the front—provided that the front does indeed intersect the beam. Smaller dilations result in the identification of small aerosol plumes associated with surface sources. Figure 6 shows one scan from the lidar at 19:21:47 UTC with the location of the front as determined from the wavelet algorithm using a 1 km dilation.

For the results shown here, we applied the wavelet algorithm in the radial component of the native spherical coordinate system of the lidar data (e.g. along each beam). Therefore, the algorithm locates the edge of the gust front as long as the boundary is not oriented at approximately parallel to a ray. As shown in Fig. 6, the algorithm fails to accurately delineate the edge of the gust for a narrow range of angles. In the future, the wavelet algorithm could be applied to lidar data interpolated to a Cartesian grid to avoid this problem.

The goal of applying the wavelet algorithm is to objectively identify the leading edge of the gust front. If this can be done, then a detailed position of the front can be

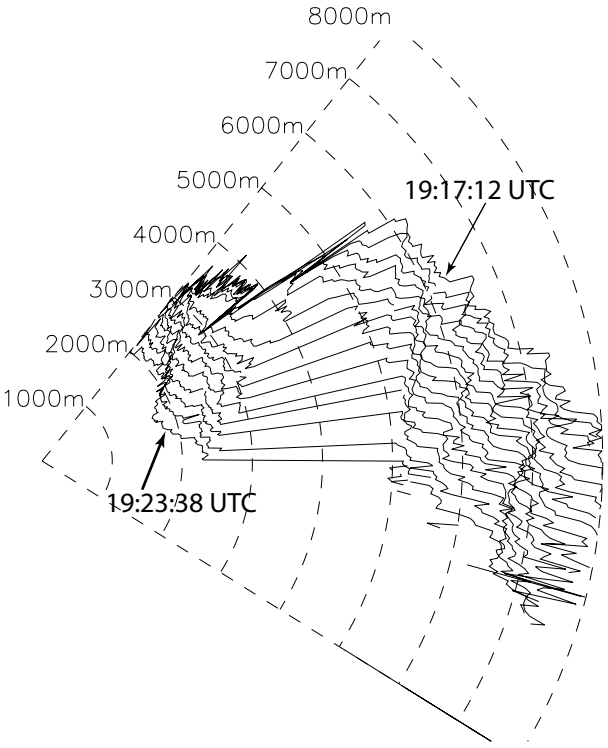

Figure 7: Location of the gust front as determined by the wavelet algorithm on each of 15 lidar scans between 19:17:12 and 19:23:38 UTC.

determined on every scan. This information can be used to calculate the velocity and changing shape of the front over time. The data may also be useful in of studies of entrainment across the frontal boundary. Figure 7 shows the gust front location as determined by the wavelet algorithm on 15 successive scans.

3.2 Wind Vectors

We applied the correlation method to derive horizontal vector motion of the aerosol structure. This technique was described by Sasano et al. (1982) and Mayor and Eloranta (2001). Although similar in approach to Mayor and Eloranta (2001), the software used to derive flow vectors for the REAL data is entirely new, incomplete, and untested at the time of this writing. We present first results here to document progress and demonstrate the new capability for future applications. The key advancement over Mayor and Eloranta (2001) is that the software has been entirely re-written in the QT4 programming language. This allows it to be compiled for operation on different operating systems and to take advantage of multiple CPUs when available. Most importantly, with a sufficiently fast computer, the software now has the ability to operate in real-time and produce vector fields that are updated on every scan. This will have value in the prediction of dispersion of aerosol plumes. To complete the software, the steps of temporal median filtering of the images, histogram normalization of the tiles, and fitting a surface to the correlation function are under development. Figure 8 shows one frame of output from the current version of the software. Vectors were computed for 700 m x 700 m tiles. When complete we expect to eliminate all low confidence velocity estimates and provide a robust method of extracting the velocity field.

The correlation technique has the advantage over Doppler lidar radial velocities that it can detect the tangential component of motion in the spherical coordinate system. It has the disadvantages, however, of coarser spatial and temporal sampling, and it relies on inhomogeneities in the aerosol scattering. When complete, this software and lidar system will be capable of providing vector motion fields on either side of the front and show the vector motion of aerosol plumes. By combining with the gust front position as described in section 3.1, detailed analysis of the kinematics and dynamics of gust fronts should be possible.

4. CONCLUSIONS

The NCAR Raman-shifted eye-safe aerosol lidar observed the passage of a well-defined gust front on 7 May 2004 in Washington D.C. A subset of the horizontal scans collected during the event are presented and

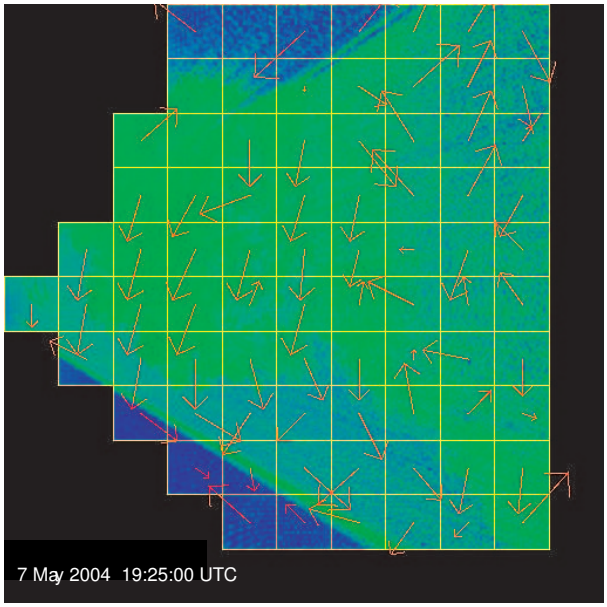

Figure 8: Preliminary aerosol motion vectors as derived from the correlation technique. Development of this algorithm and software is in progress at NCAR and the results shown are not final.

preliminary analysis started. Wavelet algorithms were applied to objectively delineate the front on each scan. Determination of frontal position on each scan allows one to accurately calculate frontal velocity. In addition to shape, location, and velocity of the frontal boundary, correlation techniques can be applied to the data to provide vectors indicating the air motion on both sides of the front. The development of this software is currently in progress at NCAR. Collectively, these tools may be used to advance understanding of gust front propagation and improve short-term predictions. In the future, by collecting both horizontal and vertical scans in an interleaved fashion, a more comprehensive and 3-dimensional visualization of gust fronts and similar density currents will be possible.

The NCAR REAL is available for use by the university community. For more information on how to request it, please contact the NSF's Division of Atmospheric Sciences or the lead author. For more information on the instrument and other data examples including animations, please go to www.lidar.ucar.edu.

Acknowledgements

NCAR is sponsored in part by the National Science Foundation. Robert Rilling, Joseph Van Andel, and Gordon Farquharson assisted with lidar data processing. Anna Petrova-Mayor assisted with the type-setting of this paper.

REFERENCES

Dabberdt, W. F., T. W. Schlatter, F. H. Carr, E. W. J. Friday, D. Jorgensen, S. Koch, M. Pirone, F. M. Ralph, J. Z. Sun, P. Welch, J. W. Wilson, and X. L. Zou, 2005: Multifunctional mesoscale observing networks, *Bull. Amer. Meteor. Soc.*, **86**, 961–982.

Davis, K. J., N. Gamage, C. R. Hagelberg, C. Kiemle, D. H. Lenschow, and P. P. Sullivan, 2000: An objective method for deriving atmospheric structure from airborne lidar observations, *J. Atmos. Ocean. Technol.*, **17**, 1455–1468.

Fujita, T. T. and F. Caracena, 1977: Analysis of 3 weather-related aircraft accidents, *Bull. Amer. Meteor. Soc.*, **58**, 1164–1181.

Liu, C. H. and M. W. Moncrieff, 1996: A numerical study of the effects of ambient flow and shear on density currents, *Mon. Wea. Rev.*, **124**, 2282–2303.

Marks, G. B., J. R. Colquhoun, S. T. Girgis, M. H. Koski, A. B. A. Treloar, P. Hansen, S. H. Downs, and N. G. Car, 2001: Thunderstorm outflows preceding epidemics of asthma during spring and summer, *Thorax*, **56**, 468–471.

Mayor, S. D. and E. W. Eloranta, 2001: Two-dimensional vector wind fields from volume imaging lidar data, *J. Appl. Meteor.*, **40**, 1331–1346.

Mayor, S. D. and S. M. Spuler, 2004: Raman-shifted eye-safe aerosol lidar (REAL), *Appl. Optics*, **43**, 3915–3924.

Mayor, S. D., S. M. Spuler, B. M. Morley, S. C. Himmelsbach, R. A. Rilling, T. M. Weckwerth, E. G. Patton, and D. H. Lenschow, 2007a: Elastic backscatter lidar observations of sea-breeze fronts in Dixon, California, in *7th Conf. on Coastal Atmospheric and Oceanic Prediction and Processes*, AMS.

Mayor, S. D., S. M. Spuler, B. M. Morley, and E. Loew, 2007b: Polarization lidar at 1.54-microns and observations of plumes from aerosol generators, *Opt. Eng.*, **46**, In press.

Sasano, Y., H. Hirohara, T. Yamasaki, H. Shimizu, N. Takeuchi, and T. Kawamura, 1982: Horizontal wind vector determination from the displacement of aerosol distribution patterns observed by a scanning lidar, *J. Appl. Meteor.*, **21**, 1516–1523.

Spuler, S. M. and S. D. Mayor, 2005: Scanning eye-safe elastic backscatter lidar at 1.54 microns, *J. Atmos. Ocean. Technol.*, **22**, 696–703.

Straka, J. M., R. B. Wilhelmson, L. J. Wicker, J. R. Anderson, and K. K. Droegemeier, 1993: Numerical solutions of a non-linear density current: a benchmark solution and comparisons, *Inter. J. Num. Meth. Fluids*, **17**, 1–22.

Warner, T., P. Benda, S. Swerdlin, J. Knievel, E. Argenta, B. Aronian, B. Balsley, J. Bowers, R. Carter, P. A. Clark, K. Clawson, J. Copeland, A. Crook, R. Frehlich, M. L. Jensen, Y. Liu, S. Mayor, Y. Meillier, B. Morley, R. Sharman, S. Spuler, D. Storwold, J. Sun, J. Weil, M. Xu, A. Yates, and Y. Zhang, 2007: The Pentagon Shield Field Program: Toward Critical Infrastructure Protection, *Bull. Amer. Meteor. Soc.*, **88**, 167–176.

Weckwerth, T. M. and R. M. Wakimoto, 1992: The initiation and organization of convective cells atop a cold-air outflow boundary, *Mon. Wea. Rev.*, **120**, 2169–2187.

Wilson, J. W., N. A. Crook, C. K. Mueller, J. Sun, and M. Dixon, 1998: Nowcasting thunderstorms: a status report, *Bull. Amer. Meteor. Soc.*, **79**, 2079–2099.